International Journal of Disaster Risk Reduction 129 (2025) 105768

Contents lists available at ScienceDirect

International Journal of Disaster Risk Reduction

journal homepage: www.elsevier.com/locate/ijdrr

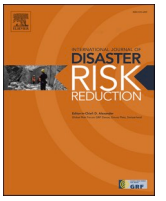

Numerical analysis of mitigation measures to reduce the pore water pressure beneath a raft foundation during real river floods

Eliana Paola Graterol [a,*], José G. Gutiérrez-Ch [a], Luis Mediero [b], Salvador Senent [a]

[a] Department of Soil Morphology and Engineering, E.T.S.I. de Caminos, Canales y Puertos, Universidad Politécnica de Madrid, c/ Prof. Aranguren, 3, Madrid, 28040, Spain
[b] Department of Civil Engineering: Hydraulics, Energy and Environment, E.T.S.I. de Caminos, Canales y Puertos, Universidad Politécnica de Madrid., c/ Prof. Aranguren, 3, Madrid, 28040, Spain

ARTICLE INFO

Keywords:
Pore water pressure
Raft foundation
Flood mitigation measures
River floods
Numerical models

ABSTRACT

Building structures in areas subjected to extreme conditions, such as river floods, is highly dependent on the ability of the raft foundation to resist significant changes in pore water pressure (PWP). Such changes, caused by rising water tables and soil saturation, can compromise structural integrity by inducing displacements and failures at the raft foundation. In this context, numerical models are an ideal tool for analyzing and predicting the PWP response that acts beneath the raft foundation during a river flood event. This work explores how numerical models can simulate flooding scenarios and assess the effectiveness of different mitigation measures to reduce PWP mobilization beneath the raft foundation, offering engineers valuable risk reduction strategies and efficient solutions. To do that, numerical models based on the Finite Difference Method are developed, incorporating real river floods associated with various river regimes, such as nivo-pluvial, nival, pluvio-nival, and mixed. Furthermore, this research analyzes the response of different mitigation measures, including levees/floodwalls, waterproof diaphragm walls, and drains, to reduce the PWP mobilization beneath the raft foundation. Results demonstrate that the numerical models developed herein effectively simulate the temporal variation of PWP beneath a raft foundation during real river floods. Also, results suggest that either combining mitigation measures, such as levees/floodwalls with waterproof diaphragm walls, or using drains can significantly reduce the PWP mobilized beneath the raft foundation for all the river regimes considered. Additionally, the findings of this research suggest that levees/floodwalls are particularly more effective in mitigating PWP mobilization during short-duration flooding compared to longer-duration events.

1. Introduction

River floods represent one of the most destructive natural risks to urban infrastructure, affecting both structural stability and the safety of buildings [1,2]. During flooding events, rising water tables and increased infiltration rates along the soil profile can generate higher pore water pressure (PWP) beneath the raft foundation, compromising the building integrity [3–5]. This phenomenon not only

* Corresponding author. Department of Soil Morphology and Engineering, E.T.S.I. de Caminos, Canales y Puertos, Universidad Politécnica de Madrid. c/ Prof. Aranguren, 3. Madrid, 28040, Spain.
E-mail addresses: ep.graterol@alumnos.upm.es (E.P. Graterol), jg.gutierrez@upm.es (J.G. Gutiérrez-Ch), luis.mediero@upm.es (L. Mediero), s.senent@upm.es (S. Senent).

https://doi.org/10.1016/j.ijdrr.2025.105768
Received 12 May 2025; Received in revised form 14 August 2025; Accepted 17 August 2025
Available online 19 August 2025

affects existing buildings located on floodplains [6,7] and coastal areas [8,9] but also poses a risk to buildings that are still under construction [10].

During a flood event, one of the main consequences occurs when the PWP mobilized beneath the raft foundation exceeds the building's self-weight, causing the structure to enter a buoyant condition [11,13]. The generated PWP not only increases the risk of flotation in the structure, but can also cause long-term damage, such as deterioration of the raft foundation materials, the appearance of cracks in the raft foundation or in the diaphragm walls used for basements, etc. [14]. Thus, infiltrated water can progressively weaken the raft foundation, compromising the load-bearing capacity of the building. In extreme cases, this may lead to displacement of the entire structure [15].

The above-described problem has been evaluated through small-scale laboratory tests by several researchers [16–20]. Such works reported that changes in the hydrostatic regime of the soil profile can affect the PWP beneath the raft foundation; however, these studies assume that water flow occurs under a constant hydraulic gradient; omitting the temporal variations in PWP that typically occur during flood events. More recently, Lee and Lee [21] conducted centrifuge tests to analyze the settlement of piles and footings under cyclical and constant variations in the water table. These tests highlighted an increase in settlement for both types of foundations with increasing water table; nevertheless, the response of raft foundations in buildings with basement levels was not addressed.

As an alternative to experimental testing, the response of PWP has also been explored through numerical models. For instance, García et al. [22] used the Finite Element Method (FEM) to analyze the vulnerability of underground structures to flooding, focusing specifically on underground flow. Furthermore, Alonso-Pollán et al. [23] applied FEM to study the response of PWP beneath a raft foundation subjected to artificial variations in the water table. More recently, Graterol et al. [11,24] employed the Finite Difference Method (FDM) to analyze the temporal variation of PWP beneath the raft foundation of a building with a basement level, considering real river flood events associated with a set of flow regimes. However, despite the valuable contributions of these studies, none of them analyzed the potential benefits of flood mitigation measures to reduce the overpressures mobilized beneath the raft foundation during a real flood event.

Thus, it is essential to implement effective drainage solutions and flood protection measures to minimize the effects of rising water tables, as well as to design foundations that take these risks into account, especially in vulnerable areas [25]. In this regard, Ni et al. [26] used FEM simulations and laboratory tests to study the response of PWP beneath the raft foundation, considering the installation of drains distributed both in the raft foundation and along the diaphragm wall under seepage conditions. Similarly, Chen et al. [27] conducted FEM simulations implementing drains placed along the diaphragm wall of the building while considering a high-intensity

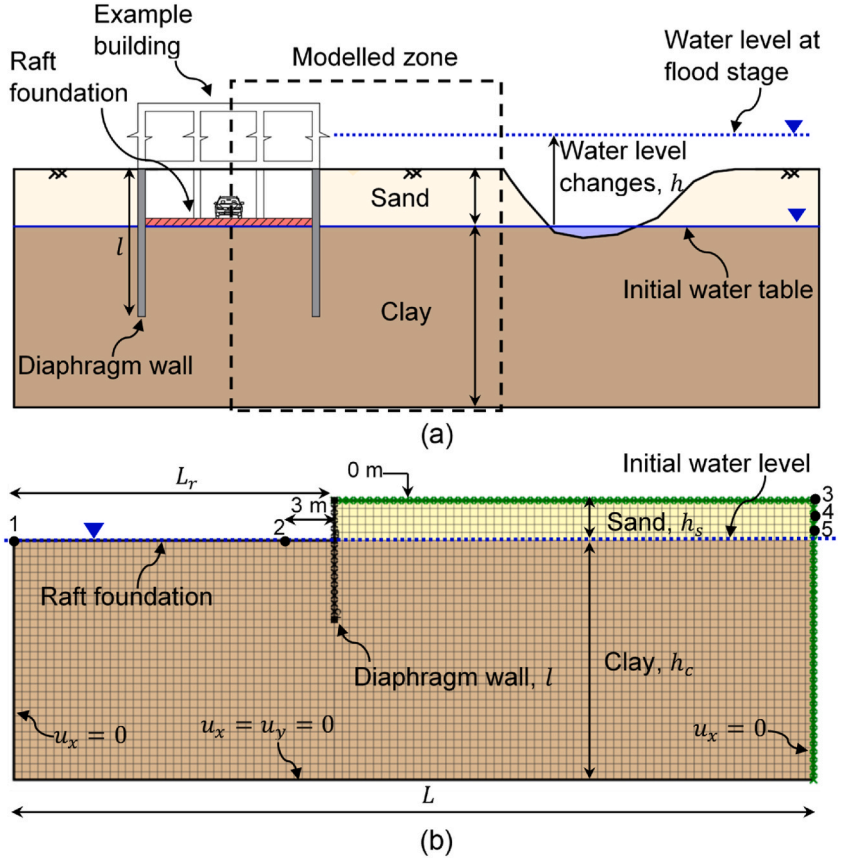

Fig. 1. Set-up of the analyzed problem: (a) conceptual model; (b) numerical model.

storm event lasting up to 48 h. Both works suggested that the incorporation of a drainage system could effectively reduce the PWP beneath the raft foundation, though they primarily focused on short-duration flood events. Additionally, Kong et al. [28] performed a statistical analysis of the probability of failure of raft foundation pumping systems in Beijing (China). They used real data on groundwater table fluctuations attributable to rainfall events over a one-year period. Their results suggested that this type of measure is effective to reduce the PWP beneath the raft foundation. In addition, its use should not be limited to periods of extreme rises in the groundwater table but it could also be applicable during any period of groundwater table variations.

Despite the advances achieved in these previous works, there are no comprehensive studies, and a more detailed investigation into the potential benefit of mitigation measures to reduce the PWP mobilized beneath raft foundations considering real regimes is still needed. This article provides a contribution in that direction by analyzing, through FDM modelling, the effectiveness of different types of mitigation measures to decrease the PWP mobilized beneath a raft foundation of a building located on a floodplain. To do that, (1) flood mitigation measures, such as levees/floodwalls, waterproof diaphragm walls, mixed mitigations, and the installation of drains, are simulated; and (2) real river flood events, both short- and long-term, associated with different river regimes –such as nivo-pluvial, nival, pluvio-nival, and mixed– are used. Subsequently, the variation of pore water pressures beneath the raft foundation is analyzed during the rainfall process, with particular attention to the maximum PWP values obtained and the effectiveness of mitigation measures.

2. Numerical modelling

This section describes: (i) the numerical models developed to simulate the influence of river floods on PWP mobilized beneath a raft foundation (see Section 2.1); (ii) the study cases and their corresponding data (see Section 2.2); and (iii) the mitigation measures used to reduce the PWP mobilized beneath the raft foundation (see Section 2.3).

2.1. Set-up of the numerical model

The 2D numerical models used in this work are built in FLAC2D commercial code [29]. The aim is to analyze the evolution of the PWP mobilized beneath the raft foundation of a building with one basement level located on a floodplain. The idealized geometry of the problem and the corresponding numerical model are shown in Fig. 1. The ground profile comprises a clay layer at the bottom and a sand layer at the top, with the water level initially located at the bottom of the sand layer. The geotechnical parameters used in the numerical simulations are listed in Table 1. Such parameters were previously validated by the Authors [30] against laboratory tests conducted by Zhang et al. [17], ensuring consistency and reliability in the present simulations. The hydraulic conductivity (k_H) in Table 1 is converted into FLAC permeability (k) and is automatically adjusted for unsaturated conditions using the cubic law $\widehat{k}(s) = s^2(3 - 2s)$, where $\widehat{k}(s)$ is the relative permeability, and s is the degree of saturation [29]. Since the sand layer is initially unsaturated ($s = 0$), its conductivity starts below the saturated value and increases dynamically as the water table rises during the simulated river flood. Thus, at each calculation step, corresponding to a given simulation time, the actual hydraulic conductivity is computed as $k(s) = k \cdot \widehat{k}(s)$. Note that, the numerical model shown in Fig. 1 is representative of an "example building" located in a flooded zone and exposed to flood events such as the one shown in Fig. 2. Taking advantage of the symmetrical building, only half of it is considered, with a raft foundation width of $L_r = 20$ m. The thicknesses of the sand and clay layers are $h_s = 2.5$ m and $h_c = 15$ m, respectively; the diaphragm wall length is $l = 7.5$ m; and the model width is $L = 50$ m (see Fig. 1b). Regarding the boundary conditions, the displacements in both the horizontal and vertical directions at the bottom of the model are fixed ($u_x = u_y = 0$), the horizontal displacement is restrained at the left and right boundaries ($u_x = 0$) and the top boundary is a free boundary. Also, the horizontal displacement of the diaphragm wall is restrained while the base that represents the raft foundation remains free (see Fig. 1b).

To simulate the influence of river floods on water tables and soil saturation, the PWP of the nodes on the right boundary and upper face of the model (green points in Fig. 1b) are modified based on the water table change–time curve recorded during real flood events (see Section 2.2). Throughout the simulation process, PWP changes are recorded at two points: points 1 and 2 located in the center and near the corner of the raft foundation, respectively (see Fig. 1b). Further details of the developed numerical model are described in Ref. [11], and for the sake of brevity, are not repeated here.

2.2. Study cases and data

The river flood events considered in the study correspond to different regions of Spain where fluvial floods can occur, and whose effects on buildings located on floodplains can be important (like the flood shown in Fig. 2). Flood hydrographs in such events were recorded at a set of streamflow gauging stations by the Automatic Hydrological Information System (SAIH, *Sistema Automático de Información Hidrológica* in Spanish) of the Ebro River Basin Authority in Spain. The gauging stations considered in the study are located

Table 1
Input geotechnical parameters used in numerical models (Graterol et al., 2024a).

	Saturated density, ρ_{sat} (kg/m^3)	Young's modulus, E (MPa)	Poisson's ratio, ν	Permeability, k (m/s)	Initial grade of saturation, s
Sand	2020	25	0.30	5.35×10^{-5}	0
Clay	2104	40	0.25	7.11×10^{-8}	1

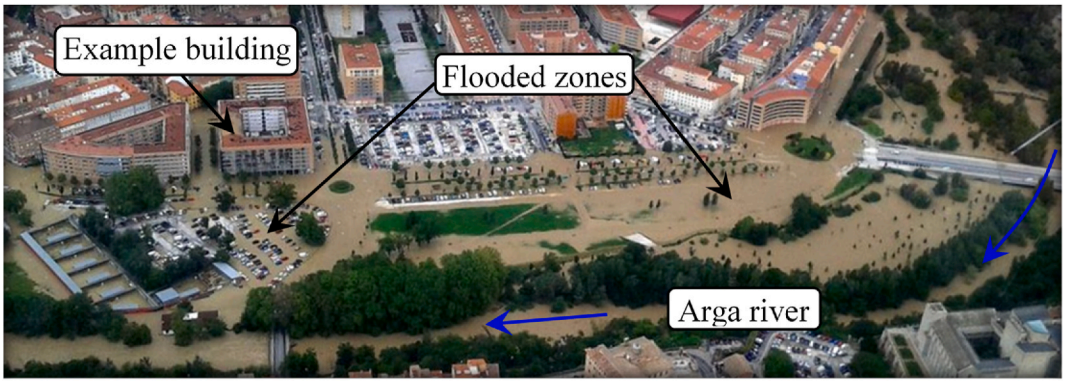

Fig. 2. Rochapea neighborhood in the flood event registered in the Arga river in Pamplona (Spain) in June 2013 (modified from Ref. [12]).

in the Spanish cities of Pamplona, Boltaña, Miranda, and Zaragoza. Such events are characteristic of four different river flow regimes: nivo-pluvial in a medium-sized catchment (500 km^2), nival in a medium catchment (700 km^2), pluvial-nival in a large catchment (5000 km^2) and mixed in a very large catchment (40000 km^2) [24]. Water table change – time curves were provided by the SAIH system of the Ebro River Basin Authority for the period 2010–2022, with a time interval of 15 min. Subsequently, the most representative event was extracted for each river flow regime. Results of these curves are shown in Fig. 3. Mathematical functions were fitted to the water table change–time curves for each river flow regime, to facilitate input data in the FLAC model (Table 2). Note that the curves of the nivo-pluvial, nival and mixed river flow regimes were rescaled to consider the same maximum water level of 5 m for all floods. (For more details, see Graterol et al. [24]).

Next, using the equations provided in Table 2 –and depending on the river flow regime considered– the river flood is induced into

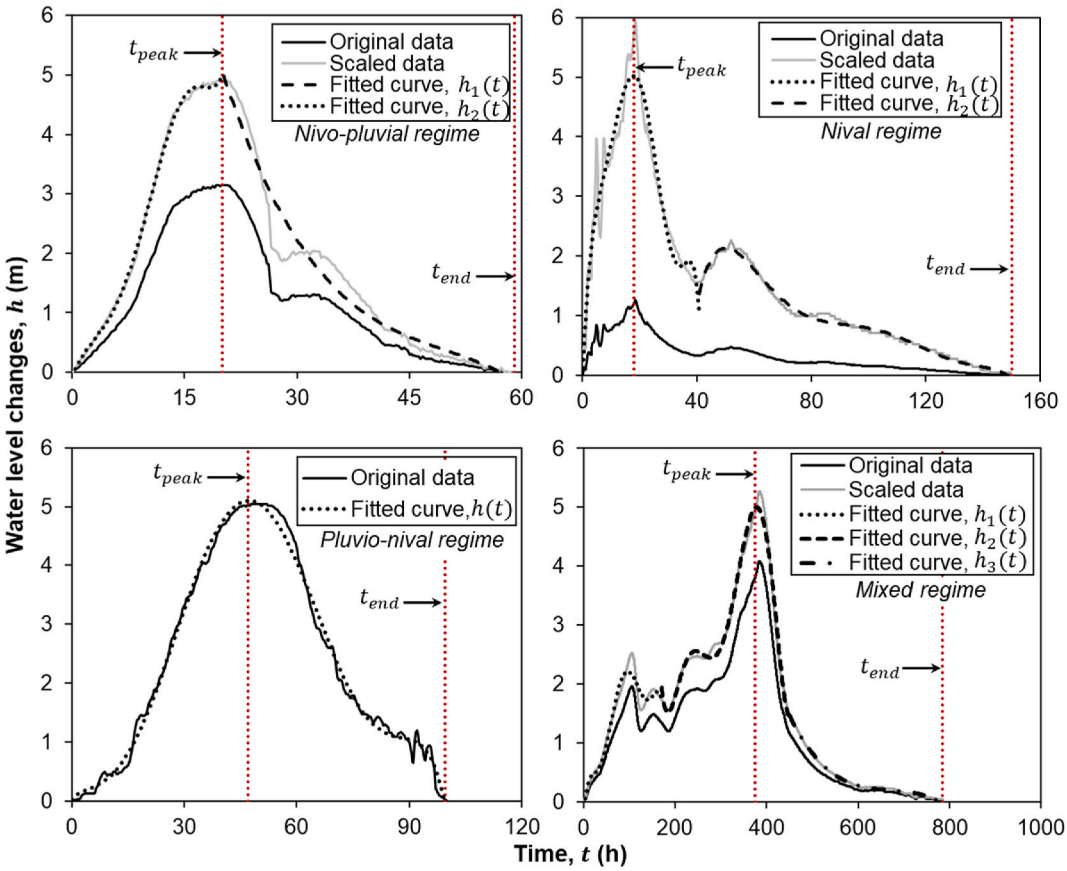

Fig. 3. Water table change – time curves during river flooding for different flow river regimes; t_{peak} represents the time in which the maximum water level of the flood occurs, and t_{end} represents the flood event end time (modified from Graterol et al., 2024).

Table 2
Equations of fitted curves for each flow regime (Graterol et al., 2024a).

Flow regime	Equation	
Nivo-pluvial	$h_1(t) = 1.455 \times 10^{-6}t^6 - 6.245 \times 10^{-5}t^5 + 6.884 \times 10^{-4}t^4 + 1.120 \times 10^{-3}t^3 - 3.224 \times 10^{-2}t^2 + 2.774 \times 10^{-1}t - 5.502 \times 10^{-2}$	Eq. (1)
	$h_2(t) = -1.295 \times 10^{-4}t^3 + 1.935 \times 10^{-2}t^2 - 1.006t + 1.849 \times 10^{1}$	Eq. (2)
Nival	$h_1(t) = -1.571 \times 10^{-7}t^6 + 1.887 \times 10^{-5}t^5 - 8.406 \times 10^{-4}t^4 + 1.727 \times 10^{-2}t^3 - 1.786 \times 10^{-1}t^2 + 1.117t - 1.180 \times 10^{-2}$	Eq. (3)
	$h_2(t) = -1.316 \times 10^{-10}t^6 + 8.110 \times 10^{-8}t^5 - 2.027 \times 10^{-5}t^4 + 2.621 \times 10^{-3}t^3 - 1.840 \times 10^{-1}t^2 + 6.591t - 9.163 \times 10^{1}$	Eq. (4)
Pluvio-nival	$h(t) = -7.632 \times 10^{-10}t^6 + 2.125 \times 10^{-7}t^5 - 2.066 \times 10^{-5}t^4 + 7.833 \times 10^{-4}t^3 - 8.565 \times 10^{-3}t^2 + 6.354 \times 10^{-2}t + 2.687 \times 10^{-2}$	Eq. (5)
Mixed	$h_1(t) = -1.459 \times 10^{-11}t^6 + 7.760 \times 10^{-9}t^5 - 1.536 \times 10^{-6}t^4 + 1.377 \times 10^{-4}t^3 - 5.505 \times 10^{-3}t^2 + 1.042 \times 10^{-1}t - 2.944 \times 10^{-1}$	Eq. (6)
	$h_2(t) = 1.841 \times 10^{-12}t^6 - 3.392 \times 10^{-9}t^5 + 2.542 \times 10^{-6}t^4 - 9.916 \times 10^{-4}t^3 + 2.123 \times 10^{-1}t^2 - 2.364 \times 10^{1}t + 2.072 \times 10^{3}$	Eq. (7)
	$h_3(t) = -1.064 \times 10^{-7}t^3 + 2.141 \times 10^{-4}t^2 - 1.442 \times 10^{-1}t + 3.271 \times 10^{1}$	Eq. (8)

the numerical model as a boundary condition. To do that, the PWP of the green nodes (see Fig. 1b) on the right and upper boundaries of the model are adjusted following the flowchart presented in Fig. 4. As indicated previously, the water table is initially located at the bottom of the sand layer (2.5 m below the surface level). This initial position represents the reference level ($h = 0$) for the water level and the water table change–time curves represent increases above this initial level. Consequently, once a 2.5 m rise is exceeded, overflow onto the ground surface occurs, and the boundary condition at the top edge of the model is modified accordingly (see Fig. 4).

2.3. Flood mitigation measures

This section describes the flood mitigation measures implemented into the numerical model to reduce the PWP beneath the raft foundation (Fig. 5). Note that all the measures considered are incorporated into the model without considering the geometry of the structural element. Instead, its effect is simulated as a boundary condition by modifying the PWP as described below (and according to the flowchart presented in Fig. 4). Therefore, the resistance of the structural element itself and the potential erosion effects driven by the river floods during its lifespan are not considered. Next, a description of each mitigation measure is provided.

2.3.1. Levee or floodwall

Levees (also known as dikes) and floodwalls (Fig. 5a) are large-scale structural elements that are employed to protect a given are

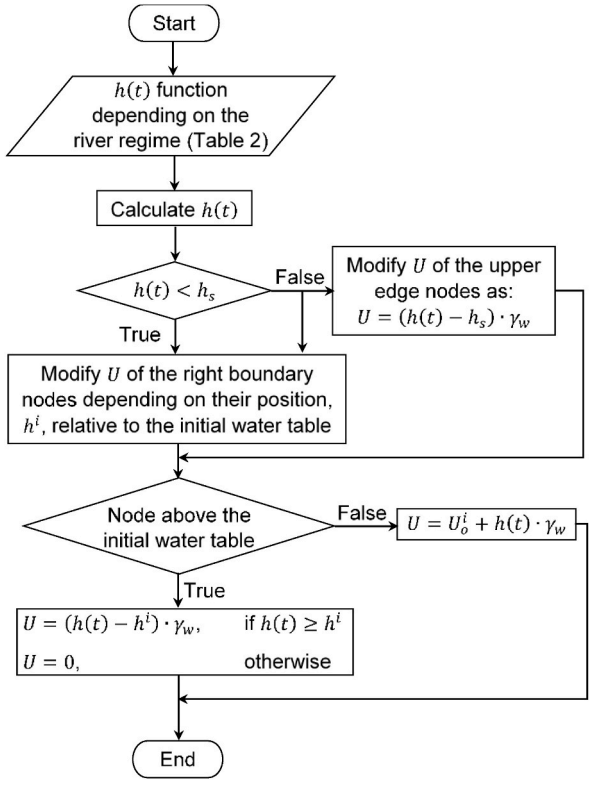

Fig. 4. Flowchart to induce the river flood flooding as a boundary condition (γ_w = specific weight of water; U_o^i = initial pore water pressure at a node i, h^i = position of node i relative to the initial water table, h_s = thickness of the sand layer).

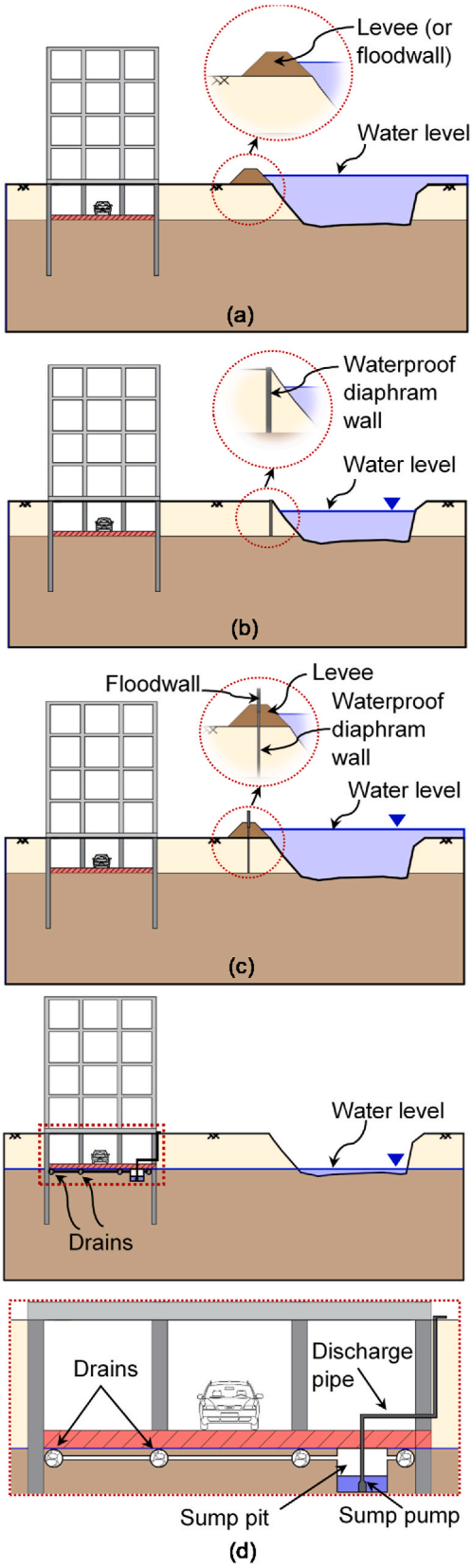

(caption on next page)

Fig. 5. Idealized representation of flood mitigation measures: (a) levee (or floodwall); (b) waterproof diaphragm wall; (c) combination of (a) and (b); (d) upper: drains, lower: close-up view of the drain locations and its associated sump system.

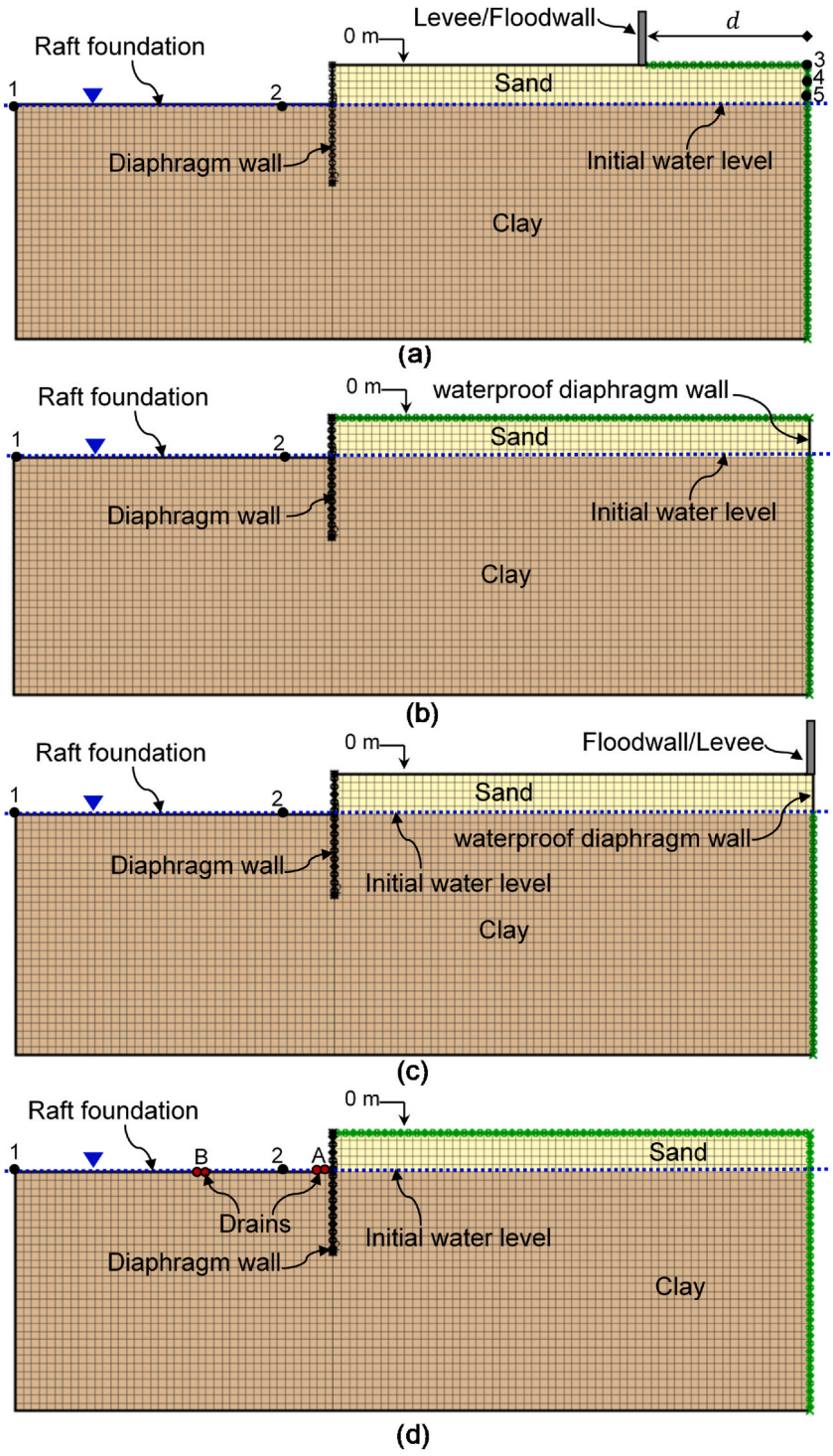

Fig. 6. Set-up of the numerical model while considering flood mitigation measures: (a) levee or floodwall; (b) waterproof diaphragm wall; (c) floodwall or levee + waterproof diaphragm wall; (d) drains (the green points represent nodes where U is modified during numerical simulations).

from flooding over long periods of time [31,32]. Therefore, such measures can protect the surrounding communities and buildings from the destructive effects of flooding [33–35]. In this research, it is assumed that the height of the levee/floodwall is higher than the maximum water level reached in the river flood (i.e., 2.5 m above the surface level or, equivalently, 5 m above the initial water table, see Fig. 3), so that flooding will not occur between the structural mitigation measure and the building. Thus, during the river flood numerical simulation, the PWP is modified at the green nodes located to the right of the levee/floodwall (see Fig. 6a). Furthermore, the effect of the levee/floodwall position on the bank of the river channel on the evolution of PWP is analyzed by varying the distance (d) between the river channel and the structural element (see Fig. 6a). In this study, $d = 0$, 5, 10 and 15 m have been considered.

2.3.2. *Waterproof diaphragm wall*

This element is commonly employed as a protection and erosion control element in areas of interest along river channels. For this purpose, pile walls are installed [36,37] or the river channel surface itself is waterproofed [38] (see Fig. 5b). In this work, this flood mitigation measure is used to reduce the groundwater flow from the river to the raft foundation [39,40]. Thus, this element is placed on the right boundary of the model, and extends in depth from the surface level to the sand-clay contact, see Fig. 5b. Its effect is simulated by leaving unchanged the PWP of the nodes in the sand layer along the right boundary. Instead, only the U values of the green nodes located at the clay layer and at the top boundary —if the water table rises above the surface level— are modified (see Fig. 6b).

2.3.3. *Levee or floodwall + waterproof diaphragm wall*

This flood mitigation measure combines the structural elements described in Sections 2.3.1 and 2.3.2 [41,42]. It is assumed that these structural elements are located at the right boundary of the model (i.e., $d = 0$ m, see Fig. 5c). Their implementation into the model is simulated by modifying only the PWP of nodes in the clay layer along the right boundary of the model (green nodes in Fig. 6c).

2.3.4. *Drains*

Finally, Fig. 5d shows an idealized representation of the last mitigation measure considered in this work. It corresponds to drains located at the raft foundation. Their function is to receive and conduct the water flow through a series of pipes to the sump pit. Subsequently, as shown in Fig. 5d, the water stored in the sump pit is discharged by a pump through a pipe for its extraction outside the building [26,27].

This mitigation measure is simulated by imposing an atmospheric pressure boundary condition (i.e. zero pore pressure) to specified nodes at the raft foundation level. This allows water to flow outward through these nodes (see Fig. 6d) [43]. To evaluate this measure, two scenarios are considered: the first considers drains through two nodes located 0.5 and 1 m from the diaphragm wall (zone A in Fig. 6d), while the second scenario contemplates additional drains through two nodes located 10 and 10.5 m away from the diaphragm wall (zone B in Fig. 6d). Note that, during the numerical simulation the water outflow at each node could be recorded.

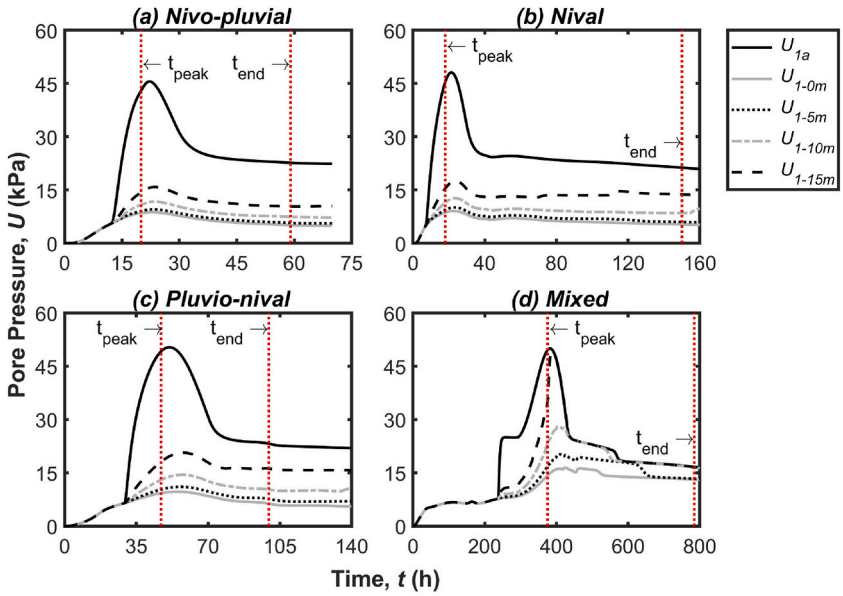

Fig. 7. Effect of a levee/floodwall on the pore water pressure, U, mobilized at the center of the raft foundation (point 1, see Fig. 1b). U_{1a} represents the U response in the absence of a levee/floodwall, while U_{1-0m} to U_{1-15m} represent the U responses with a levee/floodwall located at different distances away from the river channel, d = {0, 5, 10, 15} m, see Fig. 6a).

3. Results and discussion

Next, this section presents the results obtained in the numerical models (see Section 2.1) while considering (i) real river floods associated with a set of fluvial flow regimes (see Section 2.2) and (ii) the flood mitigation measures described in Section 2.3. (Hereinafter, the variable U will be used to refer to PWP values.)

3.1. Pore water pressure (PWP) response with a levee/floodwall

Fig. 7 illustrates the PWP mobilized at the center of the raft foundation, U_1 (see Point 1, Fig. 1b), for various distances, d, between the levee (or floodwall) and the river channel, specifically $d = 0$, 5, 10 and 15 m. For instance, U_{1-5m} corresponds to the PWP recorded at the center of the raft foundation when the levee is placed5 m away from the river channel (i.e., the right boundary of the model). Also, the PWP response without considering any type of flood mitigation measures –denoted as U_{1a}– is added to Fig. 7 for comparison.

As can be seen in Fig. 7, a levee significantly decreases the PWP beneath the raft foundation during all river floods considered herein. In particular, a notable reduction in the U values are obtained when the levee is placed next to the river channel (i.e., for $d = 0$ m, see U_{1-0m} in Fig. 7a–d). This effect is consistent, although less pronounced, for levees placed at longer distances from the river channel (i.e., $d > 0$ m) for nivo-pluvial, nival and pluvio-nival flow regimes (see U_{1-5m}, U_{1-10m} and U_{1-15m} in Fig. 7a–c). However, for the mixed flow regime (see Fig. 7d), the impact of the levee position on PWP reduction becomes less significant when the levee is placed at distances longer than 10 m from the river channel. For instance, no change in the maximum PWP mobilized beneath the raft foundation occurs when the levee is located at $d = 15$ m (see U_{1-15m} in Fig. 7d). This can be explained by the fact that, in contrast to the other river flow regimes, the flood event associated with the mixed regime has a longer duration, allowing sufficient time for the complete transmission of the PWP to the raft foundation [24]. The rise in the water level near the building (caused by flooding) and the subsequent transmission of pore pressures from the surface play a significant role in the development of PWP beneath the raft foundation. The use of levees prevents the rise of the water level in the area adjacent to the building and the corresponding increase in PWP beneath the raft foundation, as long as there is not enough time for PWP transmission, as occurs in long-duration events. Consequently, the use of levees or floodwalls is suitable for short-duration events, but their effectiveness may be reduced in longer events depending on their position.

The trend described is clearly observed when the maximum PWP for a given levee distance from the river channel is normalized by the maximum PWP without considering any type of flood mitigation measures (i.e., $U_{1,max}/U_{1a,max}$). Results of this normalization is shown in Fig. 8a. As it can be observed, a levee (or floodwall) positioned at $d = 0$ m decreases the PWP mobilized beneath the raft foundation by around 80 %, when considering short-duration river floods —associated to nivo-pluvial, nival and pluvio-nival regimes—. However, for a long-duration river flood —associated with a mixed regime— the reduction is smaller, with a decrease of

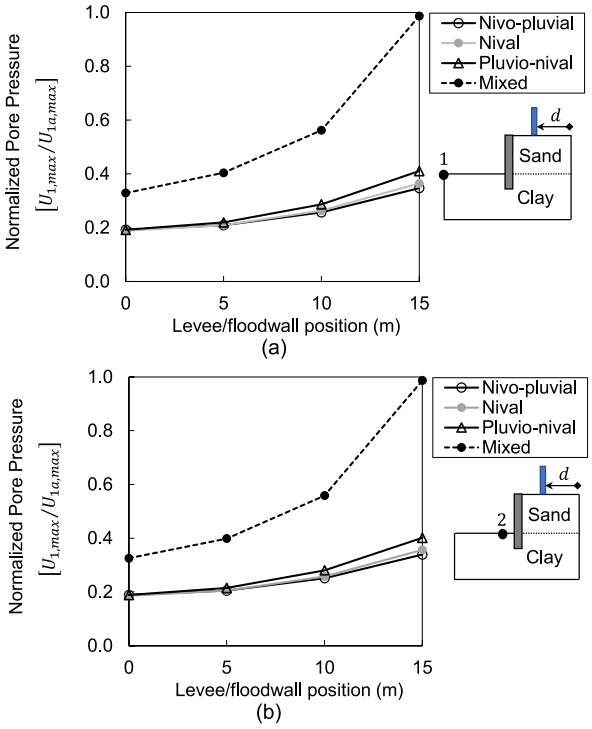

Fig. 8. Normalized pore water pressure vs levee/floodwall position: (a) at the center of the raft foundation (Point 1); (b) near the corner of the raft foundation (Point 2).

65 % of the peak PWP mobilized beneath the center of raft foundation compared with the scenario without flood mitigation measures. Furthermore, as previously indicated, the effectiveness in reducing PWP beneath the raft foundation decreases as the distances between the building and the levee (or floodwall) becomes shorter, and this type of mitigation measure is not effective for long-duration events when it is placed not far from the building. Note that, this trend is similar for the PWP mobilized near the corner of the raft foundation (see Fig. 8b).

Although less significant, the maximum PWP values for pluvio-nival events are slightly higher than those for nival events (with differences increasing with d), despite the longer duration of rainfall in the second case. This may be due to the fact that the maximum water level in the nival regime occurs earlier than in the pluvio-nival regime ($t_{peak,\text{pluvio-nival}} > t_{peak,\text{nival}}$), meaning that the decrease in PWP begins before enough time has passed for a greater pressure to be transmitted to the raft foundation. This underscores the importance of the shape of the water table change-time curve, where rapid ascents (and descents) are less dangerous than sustained rises or those occurring after a slow increase.

3.2. Pore water pressure response with a waterproof diaphragm wall

Fig. 9 shows the PWP response beneath the center of raft foundation in three scenarios: (1) without flood mitigation measures (U_{1a}); (2) considering a waterproof diaphragm wall (U_{1b}); and (3) combining a waterproof diaphragm wall with a levee (or floodwall) placed next to the river channel (U_{1c}). Results of Fig. 9 suggest that only the waterproof diaphragm wall does not contribute to a reduction in PWP recorded beneath the raft foundation during river floods. A possible reason for this is that the barrier's effectiveness is lost when the water table rises above the surface level (i.e., above the top of the waterproof diaphragm wall). At this instant, water infiltrates through the surface level, saturating the soil profile and mobilizing pore water pressures beneath the raft foundation in the same way as if no mitigation measures are used (see U_{1a} and U_{1b} in Fig. 9).

On the other hand, Fig. 9 shows that using a waterproof diaphragm wall and a levee (or floodwall) significantly reduces the U values beneath the center of the raft foundation (see U_{1a} and U_{1c} in Fig. 9). For example, it is observed that for the flood event associated with a nivo-pluvial regime, the maximum PWP decreased from 45.6 kPa to 8.8 kPa for a time of 22.2 h. This behavior occurs in a similar way to the other fluvial flow regimes, including the mixed type, whose duration is much longer. This trend might be due to, during the flood event, water flow is restricted to underground flow through the clay layer, which has low permeability. Thus, lower PWP is mobilized beneath the raft foundation.

Despite the preceding observations, a comparison between Figs. 7 and 9 reveals that the added value of the waterproof diaphragm wall is limited. The U_{1-0m} curves in Fig. 7 (levee/floodwall at $d = 0$) are nearly identical to the U_{1c} curves in Fig. 9 (levee/floodwall at

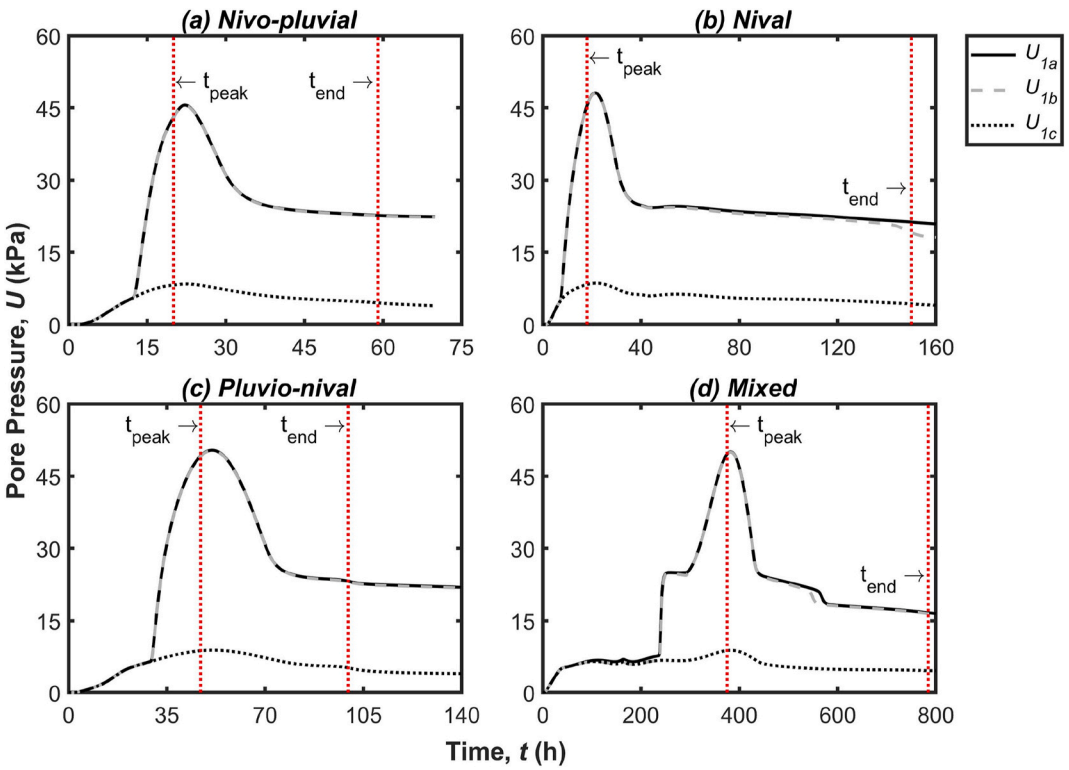

Fig. 9. Effect of a levee/floodwall + waterproof diaphragm wall (see Fig. 6c) on the pore water pressures mobilized at the center of the raft foundation (Point 1, see Fig. 1b).

$d = 0$ plus waterproof diaphragm wall). However, under the mixed regime, the waterproof diaphragm wall does demonstrate a positive effect: the maximum PWP with only the levee (U_{1-0m} in Fig. 7) exceeds that observed when both mitigation measures are employed (U_{1c} in Fig. 9). This effect appears to be related to the shape of the water table change–time curve, which shows a prolonged initial period —between 0 and 300 h— during which the water level does not exceed 2.5 m (see Fig. 3), remaining within the depth covered by the waterproof diaphragm wall. As a result, PWP transmission through the sand layer is inhibited. This once again underscores the importance of the shape of the water table change–time curve and its relationship with the channel height. Note that, as indicated in Section 2.2, the water depth–time curves have been scaled to reflect the same maximum water level of 5 m, so that flooding always occurs (whether or not it is limited by the presence of the levee/floodwall). In such cases, the effectiveness of the waterproof diaphragm wall is limited. In contrast, in scenarios without flooding, its effect could be more significant; although, in general, such scenarios are less hazardous.

3.3. Pore water pressure response with drains

Fig. 10 shows the PWP at the center of the raft foundation while considering drains as a flood mitigation measure. In Fig. 10, U_{1a} represents the response without flood mitigation measures; U_{1b}, represents the PWP response with drains located at zone A; and U_{1c}, represents the PWP response with drains located at zones A and B, simultaneously (see Fig. 6d). As can be seen in Fig. 10, the drains significantly reduce the PWP mobilized beneath the center of the raft foundation, with the effect becoming more pronounced as the number of drains increases. Note that this trend remains consistent for all river flow regimes, regardless of the flood duration.

The impact of drains on the PWP mobilized beneath raft foundation is better illustrated by normalizing the maximum PWP with drains to the maximum PWP without flood mitigation measures (see Fig. 11). As shown in Fig. 11a, placing drains in zone A results in a reduction of $U_{1\ max}$ values by around 40 % for all river flood events considered. This reduction becomes even more substantial –around 65 %– when drains are placed in both zones A and B simultaneously. A similar, yet more pronounced, effect is observed near the corner of the raft foundation (see Fig. 11), which is expected given the proximity of the drains (and particularly the drains at zone A) being closer to that corner. The detail in Fig. 11a shows that the pore water pressures in the nivo-pluvial and nival regimes are slightly higher than in the other two regimes. This may be due to the more rapid rise in water levels in these regimes, which limits the effectiveness of the drains, as PWP dissipation requires time. Nonetheless, the variations are minor, and the differences are not significant.

Furthermore, during the simulation, the total water outflow discharged at the drain points was recorded. For instance, for the river flood associated with a nivo-pluvial regime, the maximum mobilized outflow discharges (per unit model thickness) are around 0.45 l/h and 0.65 l/h at the drains located at position A and positions A and B, respectively. Similar outflow discharges were obtained for the other river flow regimes. Note that in the specific scenarios analyzed in this work, such outflow discharges can be effectively managed

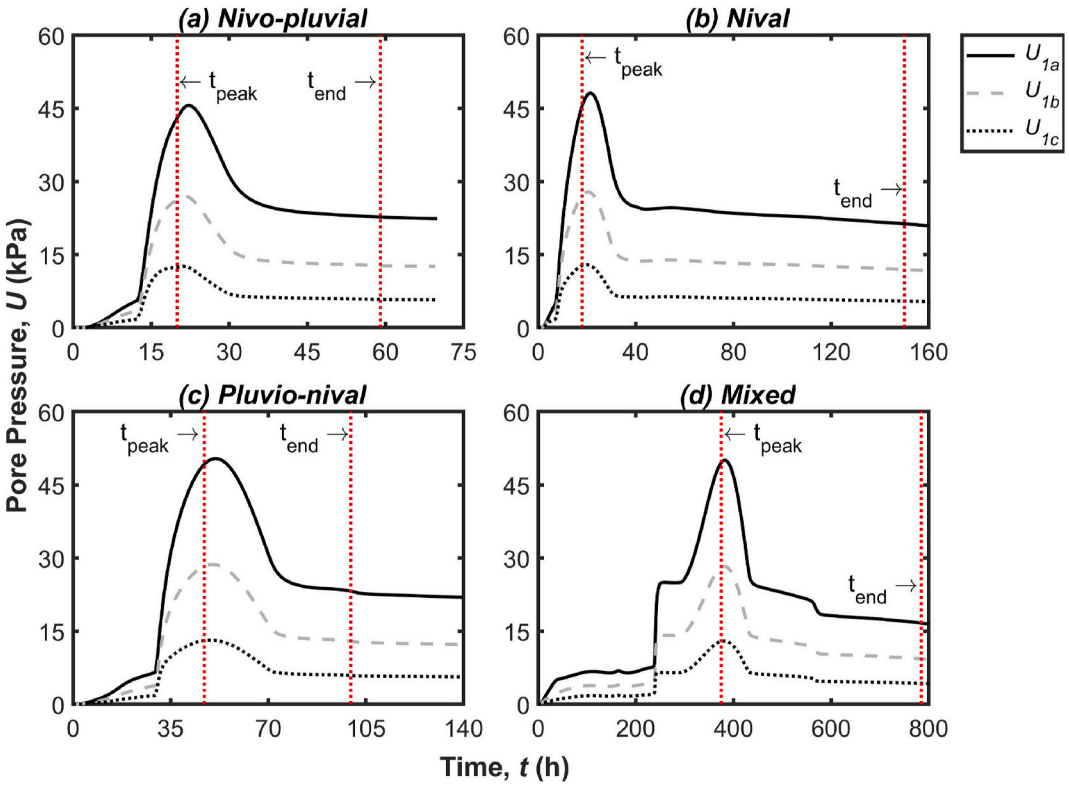

Fig. 10. Effect of using drains (see Fig. 6d) on the pore water pressure mobilized at the center of the raft foundation (Point 1, see Fig. 1b).

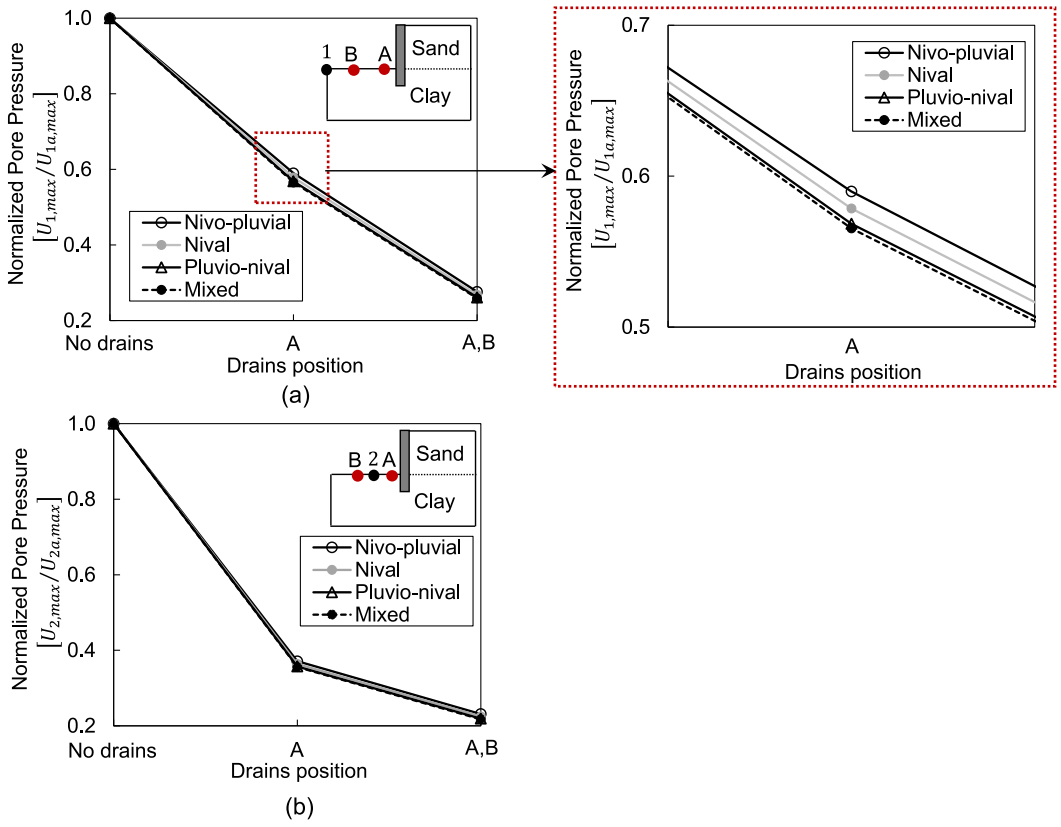

Fig. 11. Normalized pore water pressure vs drain position: (a) at the center of the raft foundation (Point 1); (b) near the corner of the raft foundation (Point 2).

by a pumping system, such as a 2-inch pipe with a pump with a total extraction rate of about 720 l/h [44]. This makes this mitigation measure feasible for implementation. However, in other situations (particularly for very short-duration floods, different geometries, or conditions where the foundation soils are already saturated) the drainage capacity should be carefully verified to ensure it can exceed the rate of water level rise.

3.4. Comparative analysis of mitigation measures

Finally, Fig. 12 shows a comparison of the normalized maximum PWP mobilized beneath the center and near the corner of the raft foundation for the different mitigation measurements. As in previous sections, the normalization is based on the ratio of the maximum PWP value recorded during the flood event with a given mitigation measure to the maximum PWP value recorded without using such a mitigation measure (i.e., $U_{1,max}/U_{1a,max}$ for point 1, for the center of the raft foundation). A value of $U_{1\ max,}/U_{1a,max} = 1$ indicates no reduction in the mobilized PWP when the mitigation measure is used. Fig. 12 also includes the river flow regimes considered and highlights the most effective results of each mitigation measure used (i.e., the levee/flodwall placed next to the river channel, the combination of the waterproof barrier and the levee/floodwall, and the use of two drains).

As can be seen in Fig. 12, the greatest reduction in the PWP mobilized beneath the raft foundation occurs when a combination of a levee (or floodwall) and a waterproof diaphragm wall is placed at the right edge of the model. This reduction is consistent across all the fluvial flow regimes considered. For instance, the reduction is 81.5 % and 82.5 % ($U_{1\ max,}/U_{1a,max} = 0.185$ and 0.175) of the maximum PWP mobilized beneath the center of the raft foundation for the nivo-pluvial and mixed flow regimes, respectively (see Fig. 12a). The second most effective mitigation measure involves using a levee (or floodwall) located at the right edge of the model; however, their effectiveness decreases for long-term fluvial flow regimes, with reductions of 81 % and 67 % of the maximum PWP observed for the nivo-pluvial and mixed flow regimes, respectively. Finally, the use of drains produces a similar trend to that observed in the combination of a levee (or floodwall) and a waterproof diaphragm wall, but with lower efficiency in reducing the PWP beneath the raft foundation –achieving reductions of around 72 % and 74 % for the nivo-pluvial and mixed flow regimes, respectively–. A similar trend is observed near the corner of the raft foundation, with greater PWP reduction when drain mitigation measures are used (point 2, see Fig. 12b), where the drains provide a more pronounced PWP reduction. As mentioned in Section 3.3, this may be due to the influence of both drain locations (zones A and B) on PWP mobilization at point 2.

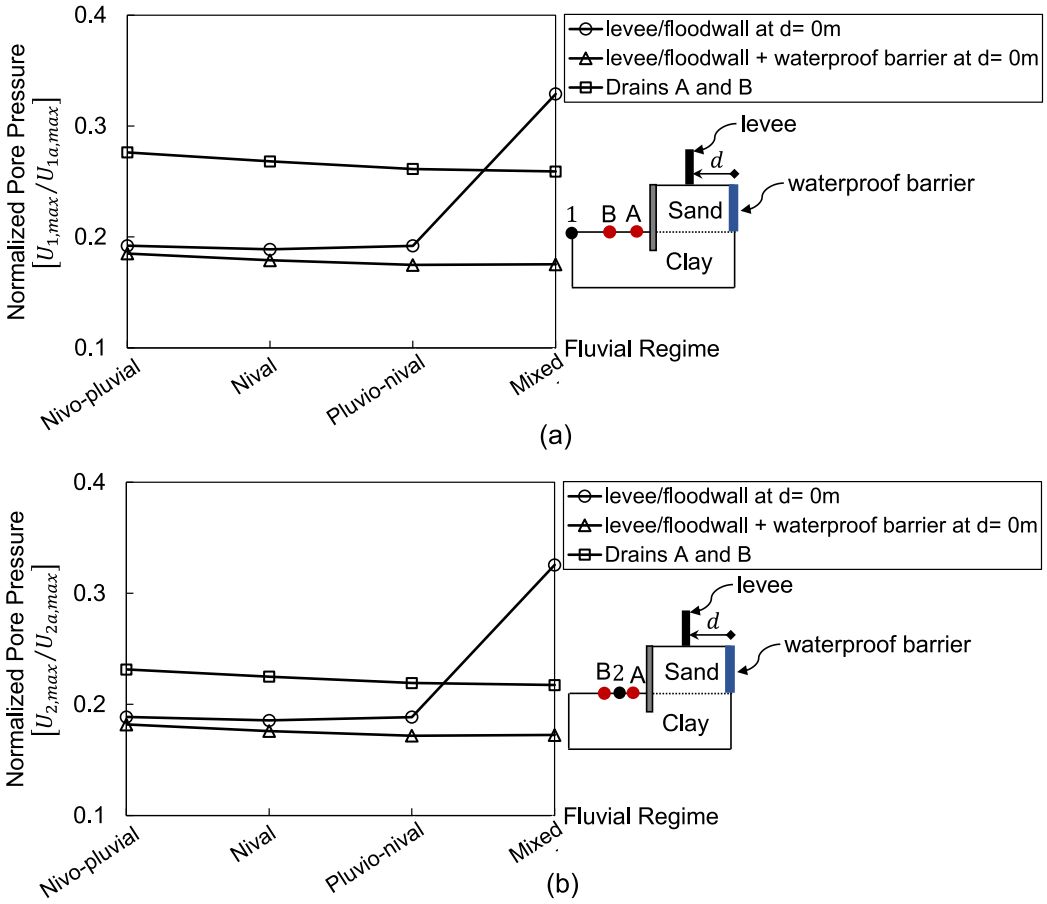

Fig. 12. Comparison of mitigation measures — normalized pore water pressure vs fluvial flow regime at the center of the raft foundation: (a) center of the raft foundation (point 1); (b) near the corner of the raft foundation (point 2).

4. Concluding remarks

Buildings located in floodplains face significant challenges, as fluctuations in the water table affect the pore water pressure (PWP) mobilized beneath raft foundations, affecting stability and safety. The overpressures generated by rising water tables and soil saturation during a flood event require accurate analysis to implement effective flood mitigation measures. In this work, novel numerical models were developed, through the Finite Difference Method and its implementation in FLAC2D, to analyze and simulate temporal variations in PWP beneath raft foundations under flooding conditions. The numerical models incorporated real data from river flood events caused by different river flow regimes. The response of the PWP was assessed when using various flood mitigation measures such as levees or floodwalls, waterproof diaphragm walls, mixed measures and drainage systems. The most significant findings are.

- Levees/floodwalls effectively prevent floodwater infiltration; however, their efficiency decreases as the distance between the building and the mitigation structure decreases, and during long-duration flood events.
- Waterproof diaphragm walls alone are ineffective once the water table rises above the surface level, but combining them with mixed measures (a levee/floodwall + a waterproof diaphragm walls) significantly improves PWP mitigation.
- Drain systems offer a cost-effective alternative for PWP reduction, as their discharged flows can be managed by conventional pumping, making them a practical option compared to large structural measures (e.g., levees/floodwalls or mixed measures).

CRediT authorship contribution statement

Eliana Paola Graterol: Writing – original draft, Software, Methodology, Formal analysis, Conceptualization. **José G. Gutiérrez-Ch:** Writing – review & editing, Software, Methodology, Formal analysis, Conceptualization. **Luis Mediero:** Writing – review & editing, Supervision, Methodology, Funding acquisition, Conceptualization. **Salvador Senent:** Writing – review & editing, Supervision, Methodology, Funding acquisition, Conceptualization.

Funding sources

This research was funded by the Spanish Ministry of Science and Innovation under grants PID2024-161402OB-I00 and PID2019-107027RB-I00, and by the José Entrecanales Ibarra Foundation through a PhD research fellowship awarded to the first author (2022–2024).

Declaration of competing interest

The authors declare that they have no known competing financial interests or personal relationships that could have appeared to influence the work reported in this paper.

Acknowledgements

The authors are grateful for the financial support provided by both the Spanish Ministry of Science and Innovation and the José Entrecanales Ibarra Foundation. In addition, the authors would like to thank Dr. Hervet Jegat from Universidad de Los Andes (Venezuela) for providing valuable ideas.

Data availability

Data will be made available on request.

References

[1] A.F. Semman, T. Maqsood, S. Venkatesan, Identification of motivating factors to help decision-making to minimise flood risk by applying private mitigation measures, Int. J. Disaster Risk Reduct. 97 (2023) 104038, https://doi.org/10.1016/j.ijdrr.2023.104038.
[2] H. Liu, W. Sun, Y. Zhang, W. Zhang, F. Han, W. Su, Experimental analysis on the interaction between underground structures and sand layer underground water level change, Undergr. Space 10 (2023) 15–36, https://doi.org/10.1016/j.undsp.2022.08.006.
[3] P. Hu, Q. Zhang, P. Shi, B. Chen, J. Fang, Flood-induced mortality across the globe: spatiotemporal pattern and influencing factors, Sci. Total Environ. 643 (2018) 171–182, https://doi.org/10.1016/j.scitotenv.2018.06.197.
[4] A. Mahmoud, M. Hussien, M. Karray, M. Chekired, C. Bessette, L. Jinga, Mitigation of liquefaction-induced uplift of underground structures, Comput. Geotech. 125 (2020) 103663, https://doi.org/10.1016/j.compgeo.2020.103663.
[5] W. Sun, W. Zhang, A. Teck, R. Zhang, Experimental and computational analysis of hydraulic behavior in shallow buried structures in sand, Gondwana Res. 124 (2023) 339–350, https://doi.org/10.1016/j.gr.2023.07.014.
[6] H. Kreibich, A.H. Thieken, Assessment of damage caused by high groundwater inundation, Water Resour. Res. 44 (9) (2008) W09409, https://doi.org/10.1029/2007WR006621.
[7] Z. Ren, Q. Lu, K. Liu, P. Ni, G. Mei, Model-scale tests to examine water pressures acting on potentially buoyant underground structures in clay strata, J. Rock Mech. Geotech. Eng. 14 (3) (2022) 861–872, https://doi.org/10.1016/j.jrmge.2021.09.014.
[8] I.H. Wong, Methods of resisting hydrostatic uplift in substructures, Tunn. Undergr. Space Technol. 16 (2) (2001) 77–86, https://doi.org/10.1016/S0886-7798(01)00037-2.
[9] I.N. Flores, O. Escolero, S. Torres, G. Riquer, Inundaciones por agua subterránea en zonas costeras. Caso de estudio: acuífero de Veracruz, Bol. Soc. Geol. Mex. 66 (2) (2014) 247–261.
[10] M. Bikçe, M. Örnek, O. Faruk, The effect of buoyancy force on structural damage: a case study, Eng. Fail. Anal. 92 (2018) 553–565, https://doi.org/10.1016/j.engfailanal.2018.06.014.
[11] E.P. Graterol, J.G. Gutiérrez-Ch, L. Mediero, S. Senent, Numerical simulation of pore water pressure evolution beneath a raft foundation during a river flooding. Proceedings of the XVIII ECSMGE 2024: Geotechnical Engineering Challenges to Meet Current and Emerging Needs of Society, Lisbon, Portugal, 2024, pp. 515–519, https://doi.org/10.1201/9781003431749-74.
[12] Noticias de Navarra, Un Nuevo Colector En la Rochapea Contra Las Inundaciones, Noticias de Navarra, 2022 [online] Available at: https://www.noticiasdenavarra.com/pamplona/2022/11/16/nuevo-colector-rochapea-inundaciones-6235544.html. (Accessed 7 March 2023).
[13] M. Yang, X. Fu, H. Liu, L. Wang, Q. Li, Influencing factors, design methods, and buoyancy reduction measures for basement anti-flotation engineering, Buildings 14 (9) (2024) 3005, https://doi.org/10.3390/buildings14093005.
[14] H. Kreibich, A.H. Thieken, H. Grunenberg, K. Ullrich, T. Sommer, Extent, perception and mitigation of damage due to high groundwater levels in the city of Dresden, Germany, Nat. Hazards Earth Syst. Sci. 9 (4) (2009), https://doi.org/10.5194/nhess-9-1247-2009, 1274–1258.
[15] M.T.A. Chaudhary, Implications of rising groundwater level on structural integrity of underground structures–investigations and retrofit of a large building complex, Struct. Surv. 30 (2) (2012) 111–129, https://doi.org/10.1108/02630801211228725.
[16] P. Ni, Kang, X. Song, L.G. Mei, Y. Zhao, Model tests of buoyant force on underground structures, J. Test. Eval. 47 (2) (2019) 1216–1235, https://doi.org/10.1520/JTE20170017.
[17] J. Zhang, J. Cao, L. Mu, L. Wang, L. Li, Buoyancy force acting on underground structures considering seepage of confined water, Complexity (2019) 7672930, https://doi.org/10.1155/2019/7672930.
[18] J. Zhou, C. Lin, C. Chen, X. Zhao, Reduction of groundwater buoyancy on the basement in weak-permeable/impervious foundations, Adv. Civ. Eng. (2019) 7826513, https://doi.org/10.1155/2019/7826513.
[19] Z. Ren, P. Ni, G. Mei, Time effect of buoyant force reduction for underground structures in clays: model test and case study, Int. J. GeoMech. 20 (10) (2020) 04020185, https://doi.org/10.1061/(ASCE)GM.1943-5622.0001823.
[20] H. Guo, R. Zhou, C. Sun, Y. Lin, J. Xie, Buoyancy of underground structures and pore water pressure conduction law in silty clay strata, Heliyon 10 (1) (2024) e24256, https://doi.org/10.1016/j.heliyon.2024.e24256.
[21] J. Lee, J. Lee, Compared analysis of settlements for deep and shallow foundations with groundwater fluctuation using centrifuge tests, Bull. Eng. Geol. Environ. 83 (2024) 215, https://doi.org/10.1007/s10064-024-03722-w.
[22] García, A., Sánchez, J.A., Vasquez-Suñé, E., Garrido, E., Pérez, A., Lázaro, J.M. Fenómenos de inundación subterránea asociados a las crecidas del río Ebro en la ciudad de Zaragoza (In Spanish). Geogaceta, 57: 147–150. Sociedad Geológica de España.
[23] J.A. Alonso-Pollán, L.M. Muñoz, R. Jimenez, Reliability analysis of constant total stress foundations subjected to water table fluctuations, Numerical Methods in Geotechnical Engineer IX 1 (2018) 523–529.
[24] E.P. Graterol, J.G. Gutiérrez-Ch, L. Mediero, S. Senent, Numerical modelling of pore water pressure response beneath a raft foundation during real river floods, J. Hydrol. 638 (2024) 161557, https://doi.org/10.1016/j.jhydrol.2024.131557.

[25] S. Liu, W. Sun, W. Zhang, Y. Wang, Z. Liu, Z. Li, Y. Yang, Q. He, Z. Wu, P. Xiao, Investigation on parameters affecting reduction coefficient of groundwater buoyancy in clay layer, J. Hydrol. 638 (2024) 121560, https://doi.org/10.1016/j.jhydrol.2024.131560.
[26] P. Ni, G. Mei, Y. Zhao, Antiflotation design for water tank using pressure relief technique, Mar. Georesour. Geotechnol. 36 (4) (2017) 471–483, https://doi.org/10.1080/1064119X.2017.1337255.
[27] L. Chen, W. Wang, A. Bu, Numerical simulation study of basement water discharge pressure relief method under rainstorm condition, Building 13 (11) (2023) 2772, https://doi.org/10.3390/buildings13112772.
[28] D. Kong, Y. Guan, H. Yuan, Study on the anti-floating water level of the underground structure's comprehensive anti-floating, Structures 56 (2023) 104921, https://doi.org/10.1016/j.istruc.2023.104921.
[29] Itasca Consulting Group, FLAC, Version 8.0. User's Manual, 2016. Mineapolis, USA.
[30] E.P. Graterol, J.G. Gutiérrez-Ch, L. Mediero, S. Senent, Simulación numérica de las fuerzas de flotabilidad bajo losas de cimentación profundas, in: XI Simposio Nacional De Ingeniería Geotécnica, Mieres, Spain, 2022, pp. 263–270. In Spanish.
[31] M. Sharp, M. Wallis, F. Deniaud, R. Hersch-Burdick, R. Tourment, E. Matheu, Y. Seda-Sanabria, S. Wersching, G. Veylon, E. Durand, The International Levee Handbook, CIRIA, London, 2013.
[32] H. Zhang, Z. Zhang, E. Wang, J. Zhang, G. Zhang, P. Yue, Effect of anti-seepage measures for maintaining thermal stability under flood dike in permafrost region, Comput. Geotech. 119 (2020) 103298, https://doi.org/10.1016/j.compgeo.2019.103298.
[33] F. Klijn, H. Kreibich, H. de Moel, E. Penning-Rowsell, Adaptive flood risk management planning based on a comprehensive flood risk conceptualisation, Mitig. Adapt. Strategies Glob. Change 20 (2015) 845–864, https://doi.org/10.1007/s11027-015-9638-z.
[34] M. Mazzoleni, E. Mondino, A. Matanó, A.F. Van Loon, M.H. Barendrecht, J. Hydrol. 636 (2024) 131305, https://doi.org/10.1016/j.jhydrol.2024.131305.
[35] S. Nedala, S. Puja, L. Kempango, S. Ikendi, Assessing flood susceptibility and effectiveness of structural flood mitigation measures applied within Mubuku catchment in Rwenzori Region, Uganda, Nat. Hazards (2024), https://doi.org/10.1007/s11069-024-06843-3.
[36] US Army Corps of Engineers, Design of sheet pile walls, Engineer Manual No. 1110-2-2504 (1994). Washington, DC, Dept. of Army.
[37] Y.-F. Li, C.-K. Chen, W. Chen, Case study of GFRP as a sheet-pile wall for stream bank protection in Taiwan, Case Stud. Constr. Mater. 15 (2021) e00602, https://doi.org/10.1016/j.cscm.2021.e00602.
[38] J. Wang, J. Tang, S.H. Jiao, Seepage prevention of mining-disturbed riverbed, Int. J. Rock Mech. Min. Sci. 75 (2015), https://doi.org/10.1016/j.ijrmms.2014.10.010.
[39] D. Macdonald, Newell A.A. Dixon, A. Hallaways, Groundwater flooding within urbanised flood plain, Journal of Flood Risk Management 5 (2012) 68–80, https://doi.org/10.1111/j.1753-318X.2011.01127.x.
[40] J.M. Abboud, M.C. Ryan, G.D. Osborn, Groundwater flooding in a river-connected alluvial aquifer, Journal of Flood Risk Management 11 (4) (2018) e12334, https://doi.org/10.1111/jfr3.12334.
[41] J. Ubilla, T. Abdoun, I. Sasanakul, M. Sharp, S. Steedman, W. Vanadit-Ellis, T. Zimmie, New Orleans levee system performance during hurricane Katrina: london avenue and Orleans canal south, J. Geotech. Geoenviron. Eng. 134 (5) (2008) 668–680, https://doi.org/10.1061/(ASCE)1090-0241(2008)134:5(668.
[42] N. Stephen, Lessons Learned from Katrina and Reducing Vulnerability, Tulan University, 2014. TIDE-1220.
[43] P.F. Li, H.C. Liu, Y. Zhao, Z. Li, A bottom-to-up drainage and water pressure reduction system for railway tunnels, Tunn. Undergr. Space Technol. 81 (2018) 296–305, https://doi.org/10.1016/j.tust.2018.07.027.
[44] J.P. Powers, A.B. Corwin, P.C. Schmall, W.E. Karck, Construction Dewatering and Groundwater Control: New Methods and Applications, third ed., John Wiley & Sons, Inc, 2007.